(Received 17 March 2024, Accepted 14 June 2024, Scheduled 1 July 2024)

Outage Prediction and Improvement in 6G for UAV Swarm Relays Using Machine Learning

Hisham Khalil[1,*], Gauhar Ali[2], Saeed Ur Rahman[3], Muhammad Asim[2], and Mohammed El Affendi[2]

[1]*Department of Intelligent Systems, Faculty of Information Technology, The University of Lahore, Pakistan*
[2]*EIAS Data Science and Block chain Lab, College of Computer and Information Sciences Prince Sultan University, Riyadh 11586, Saudi Arabia*
[3]*School of Electronic Engineering, Xidian University, Xi'an, China*

ABSTRACT: The issue of signal outages in sub-THz frequency communication for future 6G networks is addressed by this research. A machine learning method is proposed, employing Random Forest and K-Means algorithms to predict the optimal frequency band and outage probabilities for UAV relays. Both space and frequency diversity are explored to enhance signal strength, and metasurface-carrying UAVs are introduced with a $16 \times 16\,\text{mm}^2$ design. This design significantly reduces the predicted outage probability from 0.1% to 0.0178%. Finally, triangular and hexagonal UAV swarm formations with metasurfaces are investigated, demonstrating improved performance through heatmap results.

1. INTRODUCTION

The growth of several new applications, including those using artificial intelligence (AI), virtual reality (VR), three-dimensional (3D) media, and the internet of everything (IoE), has resulted in an enormous amount of traffic. In 2010, there were 7.462 EB/month of mobile traffic worldwide. By 2030, this data traffic is expected to reach 5016 EB/month [1]. The significance of enhancing communication networks is demonstrated by this statistic. A civilization that operates entirely through a digital framework features fully automated and remotely controlled systems [2]. The systems with the capability of self decisions and intelligent control are gaining popularity across every aspect of life, such as AI powered business, intelligent medicine, self driving transportation, and deep space exploration. Additionally, the smart and automated systems requiring millions of sensors are incorporated in the industrial and domestics sectors.

An intelligent network that offers everything as a service (XaaS), and a fully automated life cannot be experienced with 5G networks [3]. The 5G communication system appears sufficient for current system requirements; however, the increasing use of intelligent and automation systems is driving the demand for wireless data transmission. It may be necessary to consider future upgrades to ensure the continued smooth operation of these systems. Compared to fourth-generation (4G) communications, the 5G network will offer more features and a higher quality of service (QoS) [4]. Additionally, the frequency bands of millimeter-wave (mmWave) have been efficiently utilized and managed for 5G technology, allowing for faster data transfer rates and improved network performance.

The 5G communication system did not fully consider the integration of communication, intelligence, sensing, control, and computing functions, which will be essential for supporting the upcoming wave of internet of things (IoT) and IoE applications [5]. Moving forward, a convergence of these technologies will be necessary. For example, virtual reality (VR) equipment requires data speeds exceeding the capabilities of 5G, which highlights the need for a move beyond 5G (B5G) to meet the increasing demand for at least 10 Gbps of data speeds. As a result, the design objectives for 5G's next stage have been already investigated in literature, with the technology hitting its limitations in 2030.

Recently, researchers have been focusing on the performance of 6G mobile communication and Industry 5.0. For example, in [6], the authors used a convolutional neural network (CNN) for prediction purposes in 6G communication. Other similar works have been presented by [7–10]. In another study reported by [11], the authors focused on the outage prediction of ultra-reliable low-latency communication channels. In [12], a machine learning model was used for power outage prediction, but this technique has not been applied to communication, so there is an opportunity to use this technique for 6G mobile communication.

In [13], the authors discussed the channel model for unmanned aerial vehicles (UAVs) and propagation loss, but the use of metasurface along UAV has not been discussed. In [14], the use of metasurfaces for THz with multifunctional characteristics for RADAR and other sensing applications was reported. Ref. [15] presented a design of folded dielectrics for THz applications, verifying the design through experimentation. In [16], the concept of a cell-free IoE with correlation to 6G and the use of massive MIMO was discussed.

* Corresponding author: Hisham Khalil (hisham.khalil@is.uol.edu.pk).

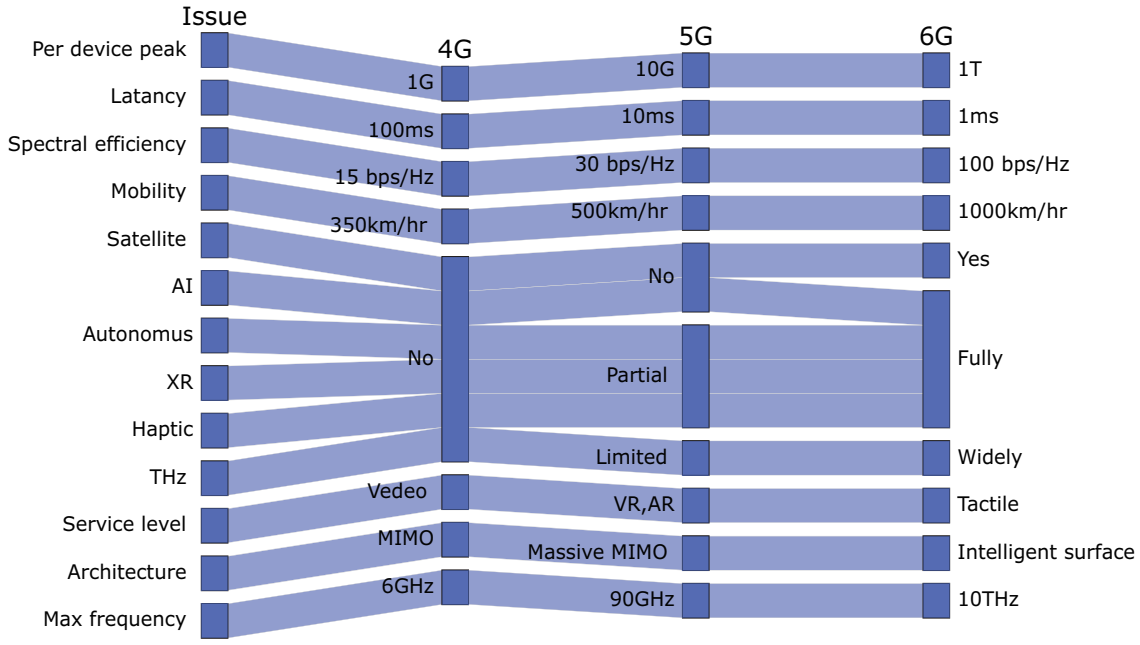

FIGURE 1. Alluvial map for feature compression of 4G, 5G and 6G.

The challenges and use cases for 6G communication were discussed by [17, 18], which presented the need and concept of beamforming for 6G, quantum communication, and the integration of AI. Beamforming is a critical function in wireless communication, and the use of antenna arrays has been found to be important for 6G network communication, as demonstrated in related works such as [19–21]. Similarly, [17] reported significant aspects of 6G, but it did not discuss hardware design considerations. In [22], a metasurface with intelligent beamforming capabilities was proposed, using a deep learning neural network. The metasurface is capable of adaptive beamforming for the 5.3 GHz frequency range, which falls under the sub-6 GHz spectrum for 5G applications [23]. In [24], a design for reconfigurable intelligent surfaces (RISs) was presented, introducing the concept of programmable metasurfaces.

The future of UAVs in cellular communication has been a topic of discussion for 5G and 6G technologies, but the design challenges have yet to be addressed [25–27]. A mathematical model for UAV-based relay was only discussed in terms of signal-to-noise ratio in [28]. According to [29], significant advancements have been made in UAV technology, with the discussion of a satellite-controlled UAV network. To the best of the authors' knowledge, no research has been published on using metasurface-equipped UAVs for predicting outages in 6G mobile communication through machine learning. Figure 1 illustrates the alluvial map for feature compression of 4G, 5G, and 6G.

This paper is structured as follows. Section 2 offers an in-depth overview of 6G technology, with a specific focus on pathloss models. In Section 3, we present machine learning-based attenuation prediction, coupled with an exploration of clustered usable frequency bands customized for 6G communication. Section 4 is dedicated to the discussion of link outage probability for UAV relay, complemented by the presentation of a contour plot illustrating space and frequency diversity. Furthermore, Section 5 focuses on the design process for a metasurface tailored to 6G networks. Finally, Section 6 explores the swarm models, as triangular and hexagonal swarm formations for 6G UAV relay systems and includes predictions for outage probability percentages.

2. MATHEMATICAL PATHLOSS FOR 6G

The mathematical model for atmospheric pathloss in 6G technology can be represented using the two-slope pathloss model, which takes into account both the line-of-sight (LoS) and non-line-of-sight (NLoS) conditions (see Fig. 2). The pathloss model can be represented as:

$$PL(d) = PL_0 + 10n\log_{10}(d) + \xi \tag{1}$$

where $PL(d)$ is the pathloss at distance d, $PL0$ the pathloss at reference distance, n the pathloss exponent, and η the zero-mean Gaussian random variable that models the log-normal

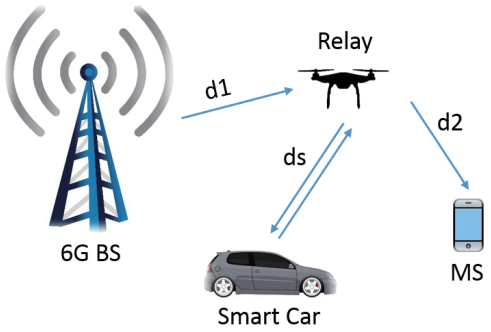

FIGURE 2. 6G communication with UAV relay model for dynamic connectivity.

shadowing effect [30]. The pathloss exponent, n, is dependent on whether the communication is in LoS or NLoS conditions. For LoS, the pathloss exponent is typically lower, whereas for NLoS, it is typically higher.

In addition to the atmospheric pathloss, 6G technology will also have to take into account other forms of signal attenuation, such as absorption and scattering by atmospheric molecules, aerosols, and hydrometeors, as well as reflection, refraction, and diffraction by the terrain. These effects can be modeled using sophisticated atmospheric propagation models, such as the Line by Line Radiative Transfer Model (LBLRTM) to accurately predict the signal attenuation and ensure reliable communication [31]. Similarly, Eq. (2) is often used to model the pathloss in free space, where the signal power decreases exponentially with distance [32].

$$T(f_o, d_o) = \exp^{-k(f_o)d_o} \tag{2}$$

In the above equation, $T(f_o, d_o)$ represents the signal power at the receiver, f_o the frequency of the signal, d_o the distance between the transmitter and the receiver, and $k(f_o)$ the frequency-dependent pathloss coefficient. The attenuation coefficient, $k(f_o)$, can be further expressed as:

$$k(f_o) = \sum_{i,j} \frac{p}{p_o} \frac{T_{stp}}{T} \times Q^{i,j} \sigma^{i,j}(f) \tag{3}$$

where p is the pressure at altitude, p_o the reference pressure, T_{stp} the standard temperature, T the temperature, $Q^{i,j}$ the water vapor density, and $\sigma^{i,j}(f)$ the absorption cross-section for the i^{th} and j^{th} water vapor absorption lines at frequency f. Moreover, the atmospheric absorption can be expressed as:

$$A_{atm}(f_o, d_o) = \frac{1}{T(f_o, d_o)} \tag{4}$$

The total pathloss is composed of two losses: atmospheric loss A_{atm} and free space scattering loss A_{spd}, which can be expressed in [32] as:

$$A_{atm}(f_o, d_o) = k(f_o)d \tag{5}$$

and

$$A_{spd}(f_o, d_o) = 20 \log_{10} \frac{4\pi f_o d_o}{c} \tag{6}$$

The total loss is the sum of Eqs. (5) and (6); therefore, the total pathloss can be represented as:

$$A_{total}[dB] = A_{atm}(f_o, d_o) + A_{spd}(f_o, d_o) \tag{7}$$

3. ATTENUATION AND BAND PREDICTION

In this section, the attenuation and usable frequency band prediction have been carried out. Machine learning has been applied once dataset has been generated.

3.1. Attenuation Prediction Using Random Forest Regression in Wireless Communication

In this section, the prediction of attenuation for millimeter wave communication was carried out using a machine learning approach. A raw dataset was first obtained from literature in picture format, and a MATLAB code was developed to extract numerical data for model training (as shown in Fig. 3) [33]. The dataset was then preprocessed to ensure accurate results during prediction.

The preprocessed data was loaded into a Python IDE, such as Jupyter Notebook, in a CSV file format. Features and labels were then extracted from the dataset. The Random Forest regression was applied for model training with a set number of estimators equal to 10. The prediction was carried out based on the trained model and achieved a 99% accuracy. The complete process is presented in Fig. 3, and the predicted result is shown in Fig. 4.

The predicted plot (Fig. 4) is in logarithmic scale, where attenuation peaks can be seen. The recommended frequency band for 6G is between 100 GHz and 1000 GHz. The machine learning prediction shows that certain frequency bands (100 to 1000 GHz) have attenuation peaks due to atmospheric effects. The first peak attenuation is observed at 120 GHz due to oxygen (O_2) absorption, and all other peaks are due to water (H_2O) molecules.

3.2. Absorption Losses Due to Water Vapor and Oxygen

In the THz wireless communication, frequency bands are categorized into low, high, and extremely high losses. The losses are a function of frequency f and are described by the equation for specific attenuation of water vapor in Eq. (8) [34]. The frequency range considered is $f < 350$ GHz, and the water vapor density is characterized at ground level with a temperature of 15°C and $\rho < 12$ g/m^3 [35].

$$\gamma_w = \left[0.067 + \frac{3}{\left(f-22.3\right)^2 + 7.3} + \frac{9}{\left(f-18.3\right)^2 + 6} + \frac{4.3}{\left(f-323.8\right)^2 + 10}\right] \times f^2 \times \rho \times 10^{-4} \tag{8}$$

The expression for the specific attenuation due to oxygen is given in Eq. (9).

$$\gamma_o = \left[\frac{7.3 r_p^2 r_t^3}{f^2 + 0.36 r_p^2 r_t^2} + \frac{0.3429 b \gamma^* o(fi)}{\left(f_i - f\right)^a + b}\right] f^2 \times 10^{-3} \tag{9}$$

where $\gamma_o^*(f_i)$ is defined as

$$\gamma_o^*(f_i) = 2.128 r_p^{1.4954} r_t^{-1.6032} \exp\left[-2.5280(1-r_t)\right] \tag{10}$$

The values of a and b are given by

$$a = \frac{\ln(\eta_2/\eta_1)}{\ln 3.5} \quad \text{and} \quad b = \frac{4^a}{\eta_1} \tag{11}$$

where η_1 and η_2 are defined as

$$\eta_1 = 6.7665 r_p^{-0.5050} r_t^{0.5106} \exp\left[1.5663(1-r_t)\right] - 1 \tag{12}$$

$$\eta_2 = 27.8843 r_p^{-0.4908} r_t^{0.8491} \exp\left[1.5496(1-r_t)\right] - 1 \tag{13}$$

where f_i is the upper limit of frequency, and r_p and r_t are constants where p represents air pressure, and t represents mean

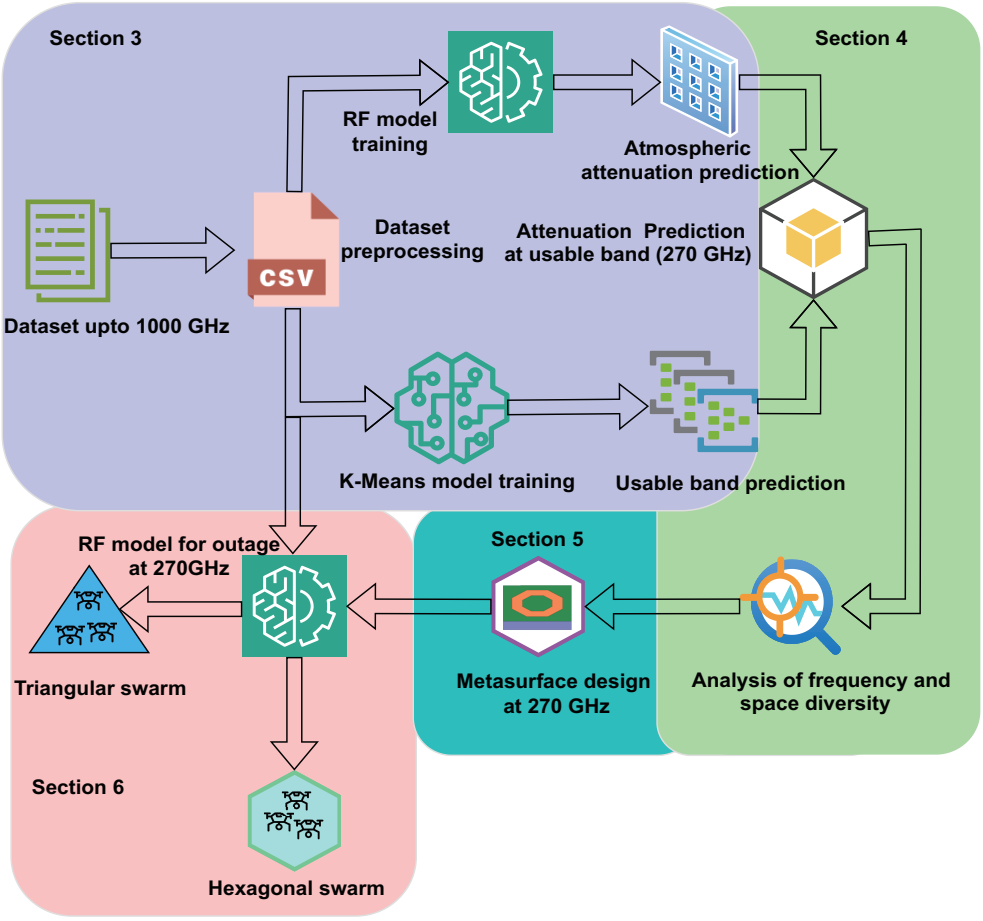

FIGURE 3. Procedure of implementation of machine learning model training and improving outage probability percentage.

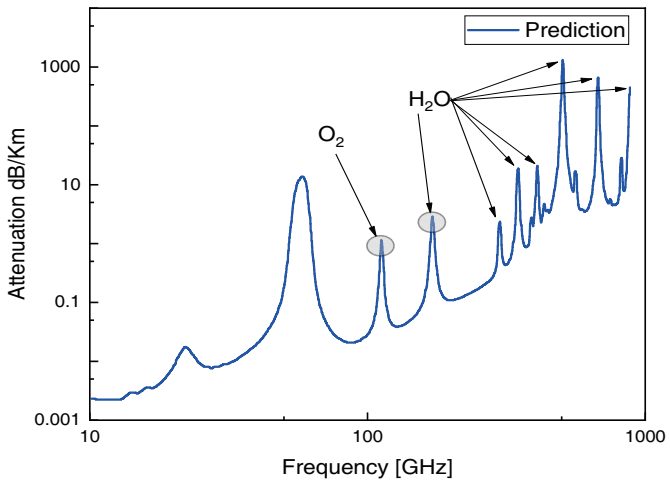

FIGURE 4. Atmospheric attenuation prediction based on machine learning model.

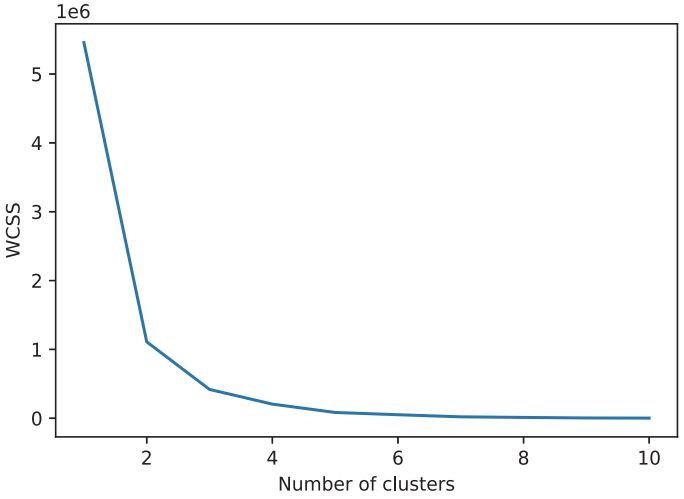

FIGURE 5. Elbow plotting for estimation k number of clusters.

temperature. The selection of the frequency band for UAV relaying systems is a crucial factor that must be carefully considered in order to ensure optimal performance. The frequency band must be chosen in such a way as to avoid high levels of attenuation due to atmospheric gases such as water vapor and oxygen, which can severely impact the quality and strength of the signal. This requires a thorough understanding of the propagation characteristics of the atmosphere at different frequencies

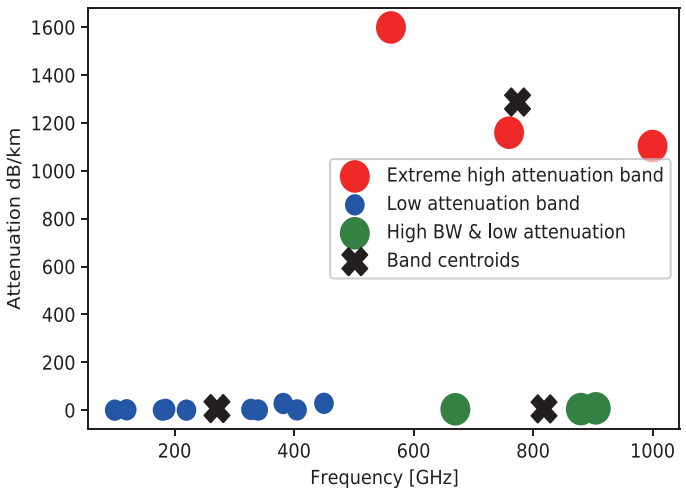

FIGURE 6. Prediction of cluster based on attenuation categories.

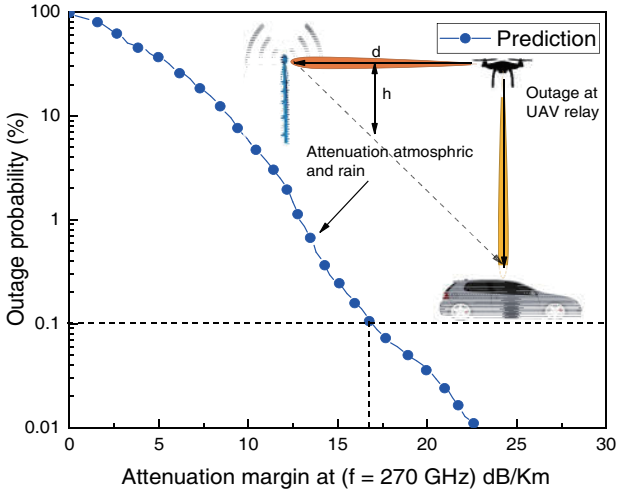

FIGURE 7. Atmospheric attenuation prediction based on machine learning model.

and the use of appropriate prediction models to determine the most suitable frequency band. The upcoming subsection has discussion of prediction model.

3.3. Prediction of Usable Frequency Band Using K-Means Clustering

The prediction of the usable frequency band for wireless communication is an important aspect of this research. In this subsection, the prediction of the frequency band that is susceptible to exceptional attenuation, caused by various atmospheric gases such as water vapor and oxygen, has been carried out. To carry out this prediction, a dataset was generated that took into account various atmospheric parameters such as temperature, pressure, and the density of atmospheric gases.

The goal was to predict the usable frequency band in the THz range and determine the level of attenuation in each band. To achieve this, a machine learning model was trained using a K-Means clustering algorithm, and the K-Means clustering performs the division of objects into clusters that share similarities. Additionally, the algorithm was applied to the dataset and generated elbow plot as shown in Fig. 5. The output of the algorithm was three categories of frequency bands, namely, low attenuation, high bandwidth, and extreme attenuation bands. The results were visualized in the form of a plot as shown in Fig. 6, where the centroids of each category were plotted for a clear demonstration of the results. The model can be used to determine the suitable frequency band and the corresponding level of attenuation [36]. From Fig. 6, the centroid of low attenuation band has been selected for further processing. On the other hand, the extremely high attenuation band cannot be used in 6G communication. The green dotted band in Fig. 6 can be used for high bandwidth and low quantitation along with hardware design challenge.

4. PREDICTING LINK OUTAGE PROBABILITY IN RELAYING UAV SYSTEM

In this section, an example setup is presented with relaying UAV for the selection of frequency $f = 270$ GHz, the centroids of low attenuation band as mentioned in the Fig. 6. According to the results shown in Fig. 6, the model is then used to select the frequency band that offers the best signal quality and strength. The frequency band with low attenuation is selected to minimize signal degradation during transmission. The frequency band is also selected based on the availability of suitable communication technology for the specific application. Additionally, the frequency band is selected to avoid interference with other communication systems operating in the same frequency range. Initially, it has been assumed that the antenna gain at relaying UAV is 35.32 dBi while the transmitting power $p_{tr} = 10$ dBm; furthermore, it is considered that the base station and relay UAV are at the same height h. Additionally, the distance for the transmission is taken as $d = 200$ m. In order to predict the link outage probability (%) at specific automation margin, a Random forest machine learning model has been trained on related dataset [37]. According to Fig. 7, the UAV relay outage probability (P_s) for frequency selective fading is formulated below:

$$P_s = 2.15\eta\left[w_m \times 10^{B_M/20} \times \frac{\tau_m^2}{|\tau_{r,M}|} + W_{NM} \times 10^{B_M/20} \times \frac{\tau_m^2}{|\tau_{r,NM}|}\right] \tag{14}$$

The multipath activity factor η may increase in the case of dynamic relay UAV. The signal bandwidth is W_x in THz, and the notch depth B_x during wave propagation is also considered. The mean delay factor is represented by τ_m, while $\tau_{r,x}$ is the reference delay used to obtain the signature. The subscript x represents both minimum phase (M) and non-minimum phase

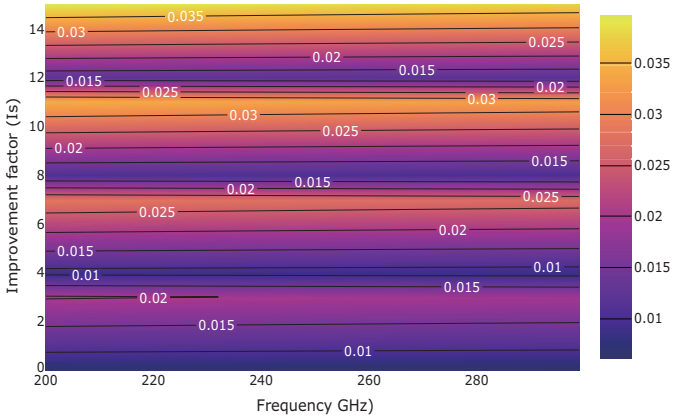

FIGURE 8. Contour plot of improvement factor with space diversity for UAV relay.

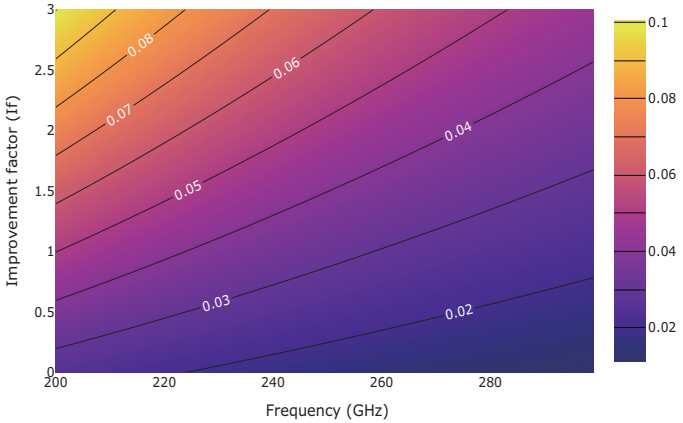

FIGURE 9. Contour plot of improvement factor with frequency diversity for UAV relay.

(NM) conditions. The details of the multipath activity parameters can be presented through an empirical equation.

$$\eta = 1 - e^{-0.2\left(P_o\right)^{0.75}} \quad \text{and} \quad \tau_m = 0.7\left(\frac{d}{50}^{1.3}\right) \tag{15}$$

Additionally, the P_o is calculated as $p_w/100$, which represents the percentage of time related to the multipath occurrence factor. To make accurate predictions of the outage probability in 6G communication, Fig. 7 can be used as a reference. By considering an attenuation margin of 14 dB/Km at the frequency of 270 GHz, this figure provides an estimate of the likelihood of an interruption in the communication link. The results are obtained using a machine learning model, which has been trained based on the various parameters affecting the communication link such as the height of the base station and relay UAV, the distance between them, the antenna gain at the relay UAV, and the transmitted power. To further improve τ_m, beamforming through ASIC is recommended as discussed in Section 2.

The outage improvement has been planned with space and frequency diversity, and the contour plot with sweeping diversity antenna on UAV has been investigated.

The contour plot in Fig. 8 provides a visual representation of the improvement in outage predictions as diversity antennas are utilized. The plot highlights the difference in predicted outage probability between the conventional setup and the one with sweeping diversity antennas. It can be observed that with the use of diversity antennas, the prediction of the outage probability becomes more accurate, and the chances of the occurrence of a 0.1% outage become less.

Similarly, the frequency diversity plot in Fig. 9 provides insight into the effect of using frequency diversity on the prediction of outage probability. By combining different frequencies, it becomes possible to reduce the predicted outage probability. The figure demonstrates the improvement in prediction accuracy when frequency diversity is utilized. The results indicate that diversity antennas can greatly enhance the precision of outage predictions, although at the expense of added weight. On the other hand, while frequency diversity also shows some improvement, it comes with an increase in hardware design complexity.

5. ENHANCEMENT OF MILLIMETER WAVE STRENGTH USING METASURFACE TECHNOLOGY

Metasurfaces have been proposed as a potential solution for improving signal strength and quality. The millimeter wave frequencies, which fall between microwaves and infrared, have unique properties that make them suitable for a range of applications such as wireless communication, imaging, and sensing. However, their propagation in the atmosphere is hindered by absorption and scattering from atmospheric gases and water vapor, which results in a significant reduction in the signal strength. Metasurfaces offer a solution to this problem by allowing precise manipulation of the electromagnetic waves at this frequency band. By controlling the phase and amplitude of incident wave, metasurfaces can be used to increase the signal strength. Furthermore, metasurface can also be designed to enhance the directivity and focus the beam which can improve the link budget and increase the communication range [38]. This makes them a promising technology for the use in 6G communication systems, imaging, and sensing applications.

5.1. Design of Metasurface

In this subsection, a metasurface has been specifically designed for a frequency of 270 GHz. The metasurface consists of an array of square-shaped unit cells arranged in a grid pattern of 16 rows by 16 columns. Each unit cell within the periodic structure is designed to have dimensions equal to the wavelength at 270 GHz, which is approximately $\lambda = 1$ mm. The meta cell has length $L = 1$ mm and width $W = 1$ mm as shown in Fig. 10. The metasurface has a total dimension of $16 \times 16\, mm^2$ with dielectric constant (ϵ_r) of 2.2, which has been simulated using the HFSS (High-Frequency Structure Simulator) software as shown in Fig. 11. The simulation results, specifically S_{21} parameter, show that the designed metasurface is capable of

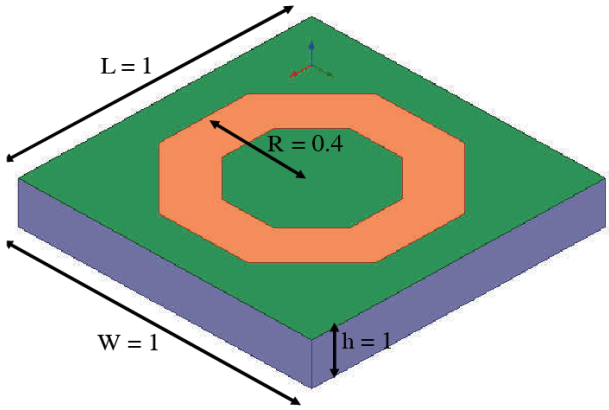

FIGURE 10. Unit cell design of metasurface for relay UAV (units in mm).

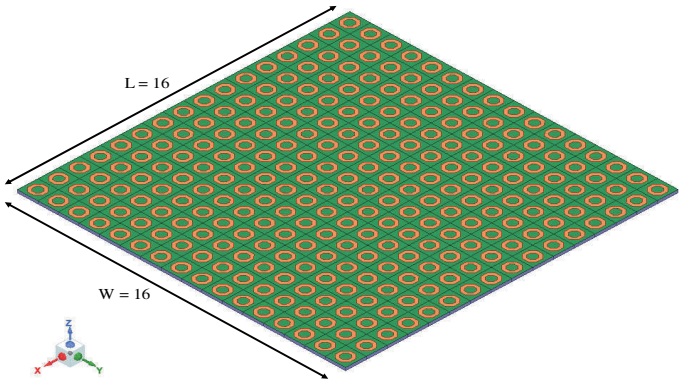

FIGURE 11. $16 \times 16\,\text{mm}^2$ grid design of metasurface for relay UAV.

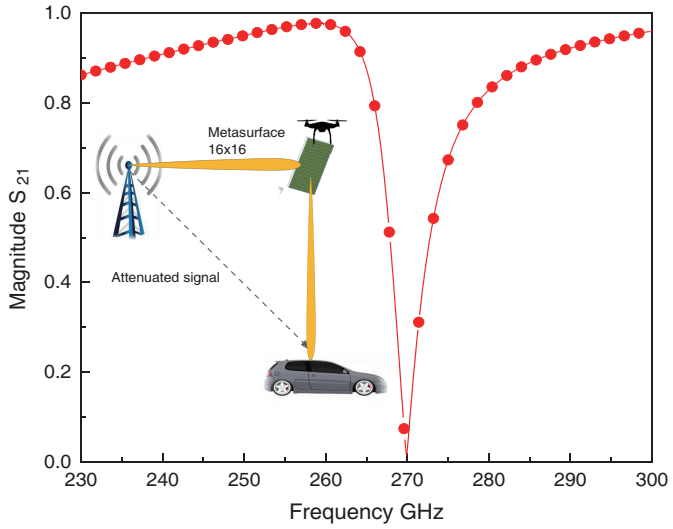

FIGURE 12. Magnitude of S_{21} scattering parameter for metasurface (16×16 grid).

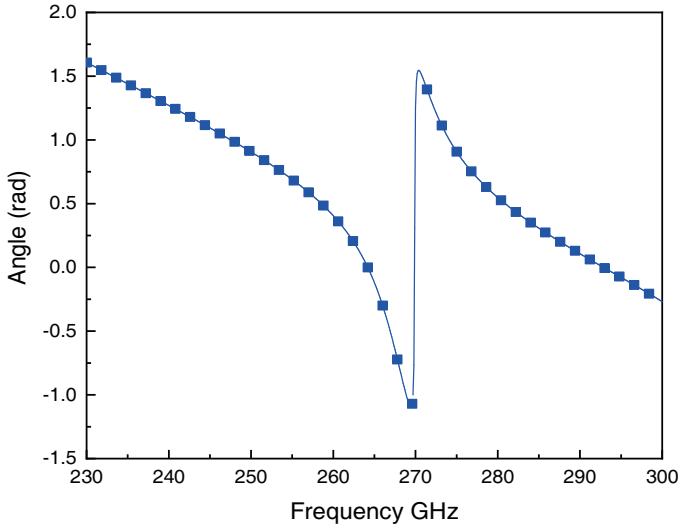

FIGURE 13. Phase of S_{21} scattering parameter for metasurface (16×16 grid).

improving the signal strength and quality of millimeter wave signals.

The metasurface design is based on the principle of subwavelength structures that can manipulate the phase and amplitude of electromagnetic waves. By carefully designing the geometry and material properties of the unit cells, the metasurface can be used to control the reflection and transmission of millimeter wave signals. The simulation results show that the metasurface is able to achieve a high transmission and low reflection, which improves the signal strength and quality of the millimeter wave.

This design can have potential applications in 6G wireless communication systems, as well as other millimeter wave applications such as imaging and sensing. With the advancement of technology in millimeter wave communication and sensing, the use of metasurfaces has emerged as a promising approach to improve the performance of these systems. This study is a significant step towards the development of efficient and low-loss metasurfaces for millimeter wave signal manipulation.

5.2. Simulation Results

The simulation results of the designed metasurface for 6G communication systems are presented in this section. S_{21} parameter, which is a measure of the transmission coefficient, was used to evaluate the performance of the metasurface. The simulation results show that the metasurface has a total gain of 5 dB. This gain is achieved through the use of the phase variation within the unit cell, which allows for constructive interference of the incoming signals.

Additionally, the metasurface was also evaluated for its ability to suppress unwanted reflections and scattering as the magnitude and phase of S_{21} are shown in Figs. 12 and 13, respectively. The results show that the metasurface has a low reflection coefficient, indicating that it effectively suppresses unwanted reflections. The scattering coefficient was also found to be low, indicating that the metasurface effectively suppresses unwanted scattering. In conclusion, the simulation results of the designed metasurface for 6G communication systems have shown that it meets the required specifications for 6G commu-

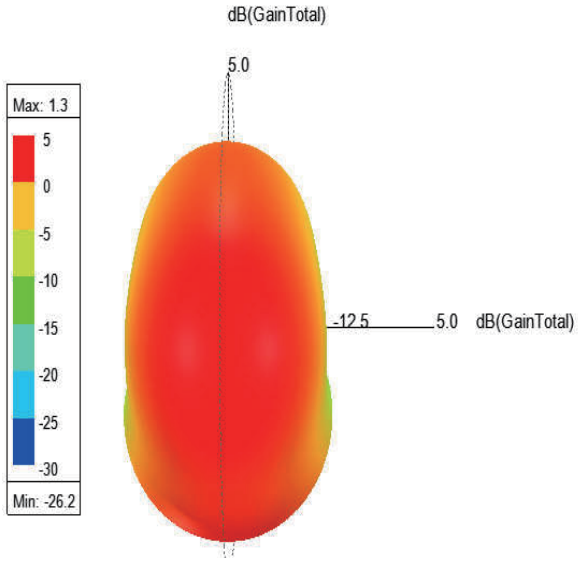

FIGURE 14. 3D polar plot of unit cell's radiation pattern showing the gain of 5 dB.

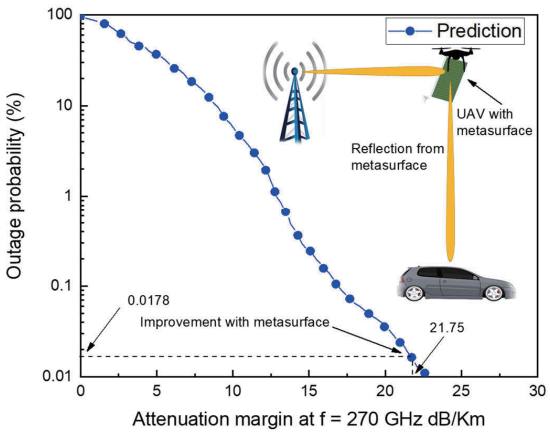

FIGURE 15. Atmospheric attenuation prediction based on machine learning model.

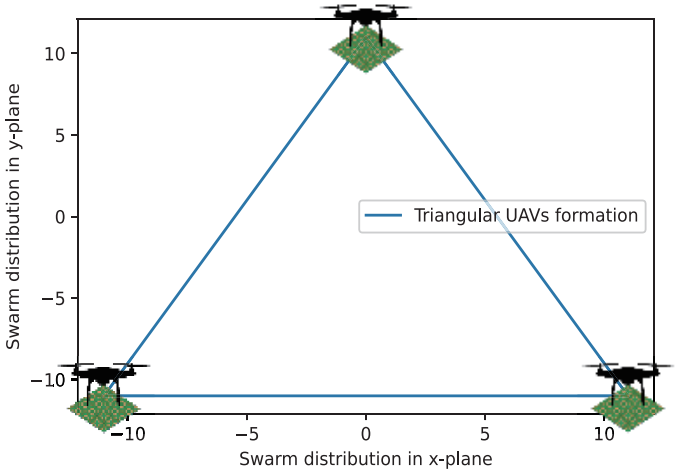

FIGURE 16. Triangular swarm formation (low resource deployment) with UAVs located at maximum attenuation margin for outage probability prediction.

nication systems. The metasurface has a total gain of 5 dB as presented in Fig. 14, low reflection coefficient, and low scattering coefficient, making it suitable for the use in a 6G communication system.

It should be noted that the above results are based on simulation, and further testing and optimization of the metasurface are necessary in order to fully evaluate its performance in a real-world scenario. Additionally, the metasurface will be carried by a UAV relay station, which can be used to improve the attenuation margin. Fig. 15 demonstrates the improvement achieved in the attenuation margin by using metasurface technology. As seen in the figure, the attenuation margin has increased from 16.75 dB to 21.75 dB, resulting in a significant improvement in the signal quality. This increase in the attenuation margin has directly impacted the prediction of outage probability, reducing it from 0.1% to 0.0178%. This decrease in the outage probability indicates a more reliable and robust communication system, which is essential for various applications such as wireless communication, imaging, and sensing. The use of metasurface technology not only improves the signal quality but also enhances the directivity of millimeter wave, which can be used to increase the communication range and link budget. Overall, the results obtained from Fig. 15 highlight the potential of metasurface technology for improving the accuracy of outage predictions in millimeter wave.

6. SWARM FORMATION FOR 6G NETWORK

According to the previous section, the attenuation margin has been improved using a designed metasurface. The following

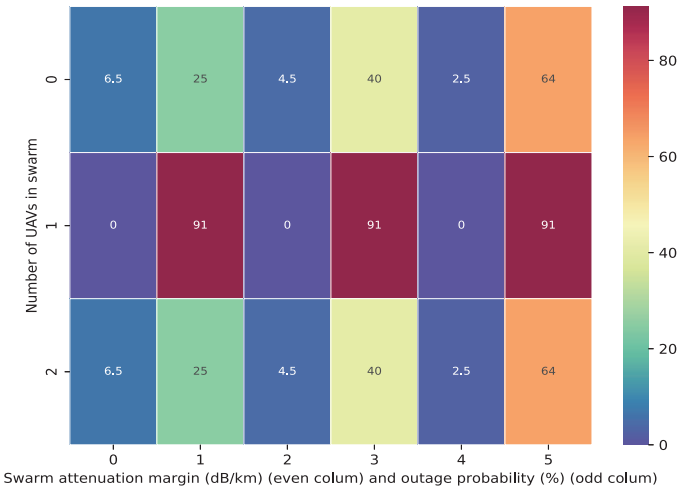

FIGURE 17. Heatmap of predicted outage probability percentage for triangular swarm without metasurfaces.

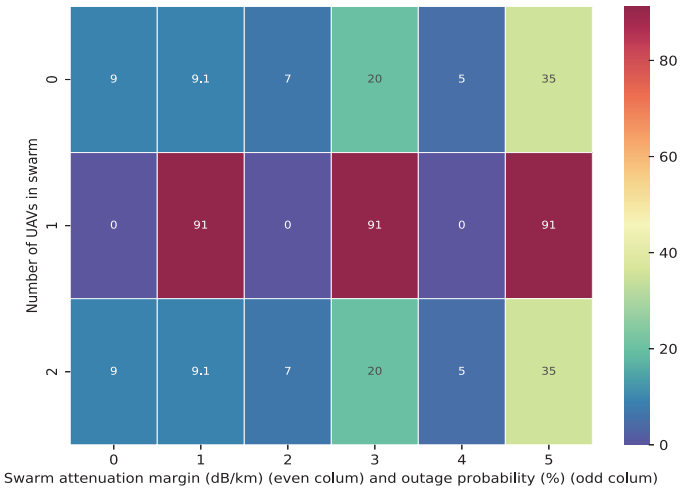

FIGURE 18. Heatmap of predicted outage probability percentage for triangular swarm with metasurfaces.

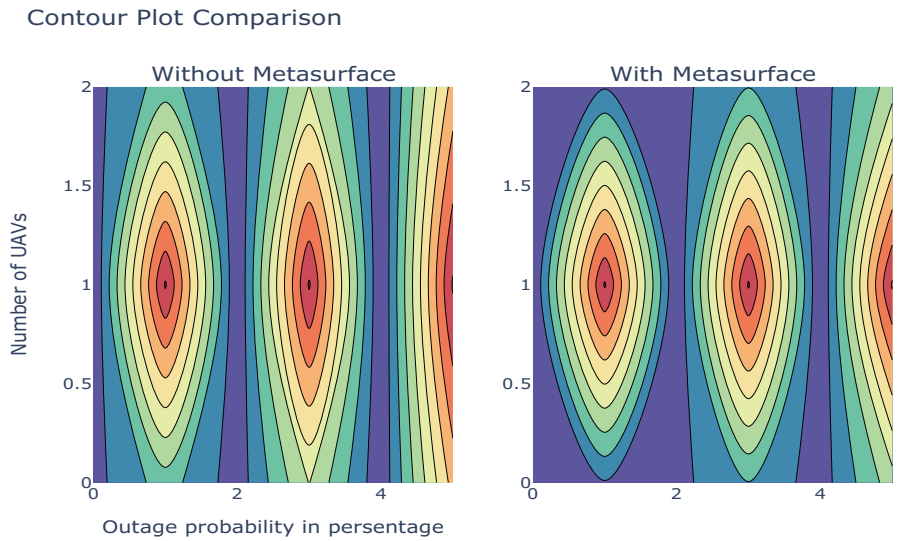

FIGURE 19. Contour plots of triangular formation without and with metasurfaces.

two subsections present the two types of UAV swarm formations aimed at improving attenuation.

6.1. Triangular UAVs Formation

In the triangular formation, three UAVs are strategically positioned at the vertices of the triangle, while the 6G-based station is centrally located within the triangular formation, as depicted in Fig. 16. Initially, the UAVs are strategically placed to maximize the attenuation margin, reaching a value of 17 dB/km. Subsequently, the UAVs are repositioned with attenuation margins of 13, 9, and 5 dB/km, respectively. Notably, in this scenario, the proposed metasurface is not employed on the UAVs. To predict the corresponding outage probability percentages, a Random Forest model has been trained. The predictions are visually represented in the form of a heatmap, as shown in Fig. 17.

On the other hand, the UAVs are positioned at the same locations, but with the deployment of a metasurface. An enhanced version of the heatmap is illustrated in Fig. 18 wherein the dark shaded area has more outage probability. For a clearer understanding of the concept, Fig. 19 presents a comparison of contour plots. Herein, the contour plot with the metasurface illustrates an improvement in the outage probability, accompanied by a shrinking of the pattern. The analysis of results reveals that in the triangular formation, there are red zones in the outage probability contour plot, indicating a significant percentage of high outage occurrences.

6.2. Hexagonal UAVs Formation

To enhance the outage probability, a hexagonal formation comprising six UAVs has been explored. Initially, the UAVs are positioned to maximize the attenuation margin (17 dB/km) without the use of a metasurface, as illustrated in Fig. 20. Additionally, the coordinates for the i-th UAV in a regular hexagonal formation with distance d between adjacent UAVs are given

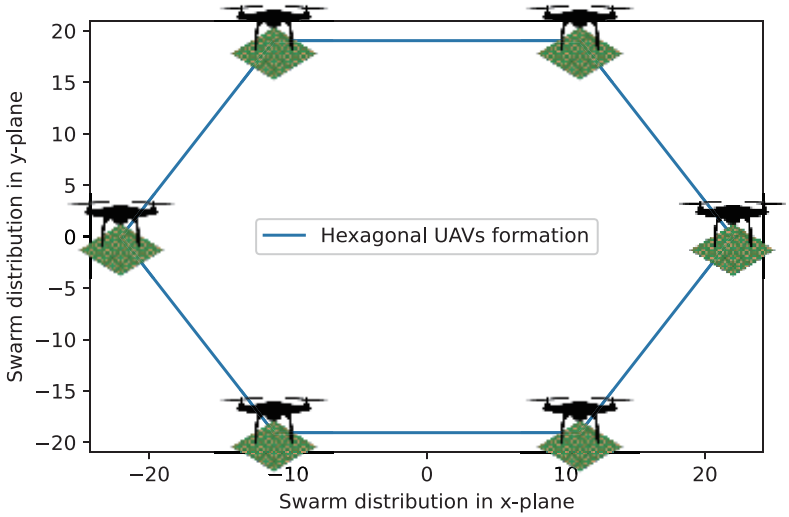

FIGURE 20. Hexagonal swarm formation (high resource deployment) with UAVs located at maximum attenuation margin for outage probability prediction.

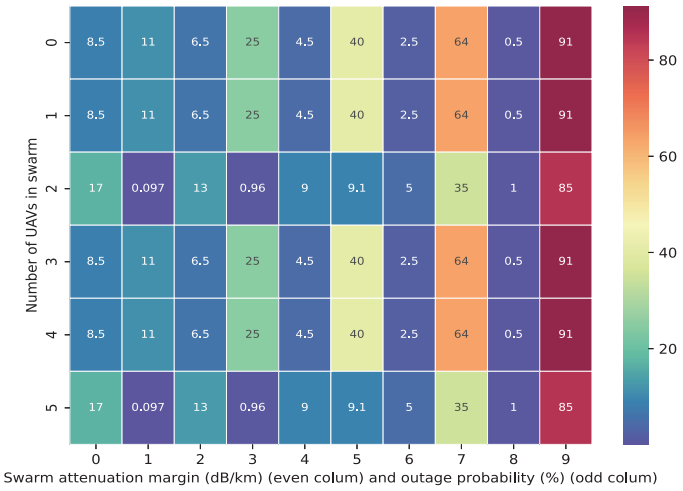

FIGURE 21. Heatmap of predicted outage probability percentage for hexagonal swarm without metasurfaces.

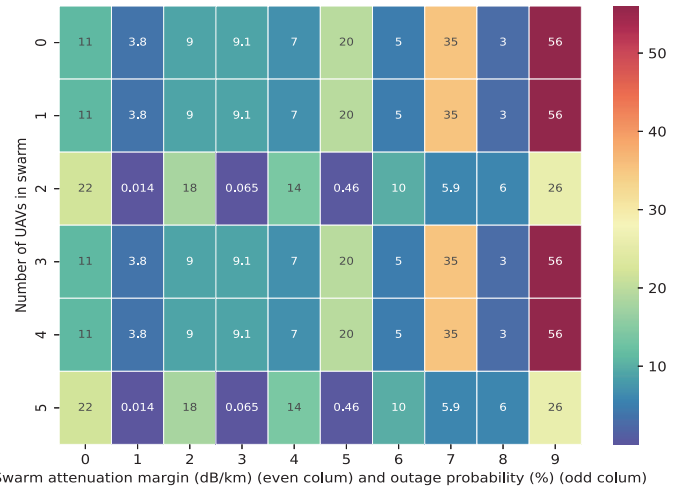

FIGURE 22. Heatmap of predicted outage probability percentage for hexagonal swarm with metasurfaces.

by:

$$H_{i,j} = (d\cos(\theta_i), d\sin(\theta_i)) \tag{16}$$

where $\theta_i = \frac{2\pi i}{6}$ represents the angular position of the i-th UAV in radians while j presents the step for attenuation margin. Similar to the triangular formation, the base station is centrally located within the hexagon, and the UAVs operate without metasurfaces. Subsequently, the UAVs' placement is adjusted in increments of 4 dB/km, and the predicted results are showcased in both heatmaps. Fig. 21 represents the scenario without metasurfaces. On the other hand, Fig. 22 displays the outcomes with the inclusion of metasurfaces. From the analysis of Figs. 21 and 22, a significant reduction in outage probability has been observed in the red color zone due to the employability of the metasurface. Furthermore, a comparison of contour plots is also presented in Fig. 23, offering a better visual assessment of the hexagonal UAVs formation outcomes.

To analyze both formations, triangular and hexagonal, the hexagonal configuration demonstrated significant improvement, especially with the incorporation of metasurfaces. This configuration successfully achieved the goal of enhancing outage probability, reaching an optimized state with an optimal number of UAVs. Notably, it achieved a remarkable 5.6% outage probability with an attenuation of 10 dB/km, and the comparison of proposed work is shown in Table 1.

In our proposed work, we have introduced a comprehensive analysis of UAVs and swarm parameters for 6G communication systems. Leveraging a combination of Random Forest and K-Means algorithms, we developed a predictive model to assess swarm outage probability. This approach aims to enhance the reliability and performance of UAV relaying in 6G scenarios, contributing to the field of interruption probability prediction through machine learning and intelligent algorithms. Additionally, Table 2 provides a comprehensive summary of the results

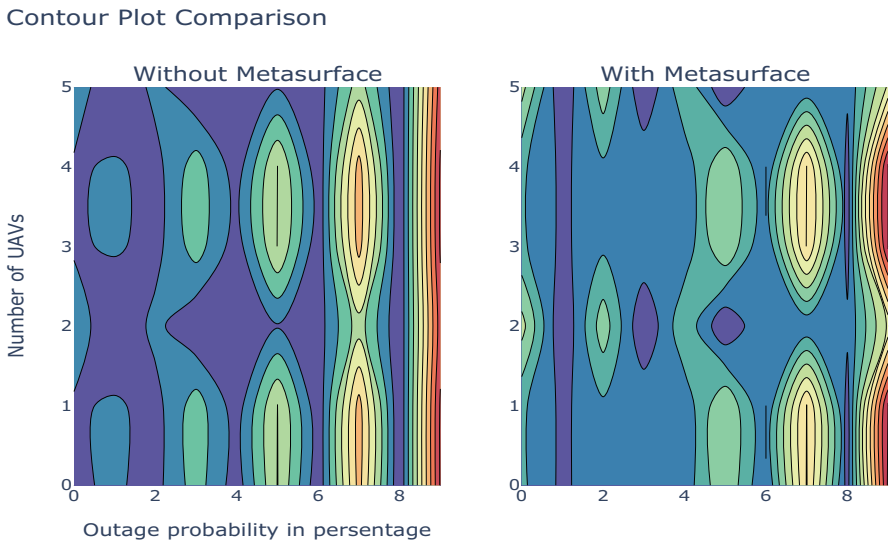

FIGURE 23. Contour plots of hexagonal formation without and with metasurfaces.

TABLE 1. Comparison of UAVs and Swarm Parameters.

Ref.	UAVs	ML & AI	Algorithm	Model	Swarm	Application
[39]	–	Yes	ML/AI	Blockchain	Yes	6G
[40]	–	Yes	ML/AI	NTN	Yes	6G
[41]	3	No	–	–	Yes	6G
[42]	1	Yes	RL	–	No	5G
[43]	1	No	Iterative algo.	–	No	–
Proposed Work	6	Yes	R.F. & K-means	Swarm Outage	Yes	6G

TABLE 2. Comparisons are made between the results of UAV triangular and hexagonal swarm formations with and without Metasurfaces (MS).

Swarm type	UAVs placement	Outage Prob. without MS	Outage Prob. with MS	Contour plot with MS
Triangular	Fig. 16 (11 dB/km)	9.1%	6.5%	Reduced red pattern (Fig. 19)
Hexagonal	Fig. 20 (22 dB/km)	0.097%	0.014%	Reduced dual red pattern (Fig. 23)

obtained from swarm formations, offering a detailed comparison between different configurations and their corresponding outcomes.

7. CONCLUSION

In conclusion, this paper has showcased the application of machine learning techniques for predicting outage probability in UAV relaying. Leveraging the Random Forest algorithm, we accurately forecasted atmospheric losses in millimeter wave signals and identified the optimal frequency band through K-Means clustering. The selected frequency band was employed to predict UAV relay outage probability. The impact of space and frequency diversity is also thoroughly investigated. Moreover, a novel metasurface design was introduced, resulting in a substantial improvement in outage prediction — from 0.1% to an impressive 0.0178%. Additionally, the compact size of the metasurface $16 \times 16\,\text{mm}^2$ played a pivotal role in enhancing the received signal strength at the UAV relay. Finally, two distinct use cases, triangular and hexagonal UAV swarm formations were discussed. The machine learning model was utilized to predict outage probability percentages, and the results were presented through heatmaps. This study not only advances the understanding of outage probability prediction in UAV relaying but also underscores the effectiveness of machine learning and metasurface design in improving reliability and performance in such communication systems. Future research could explore additional scenarios and optimizations to further refine and expand upon these findings.

ACKNOWLEDGEMENT

This work is supported by EIAS Data Science and Block chain Lab, College of Computer and Information Sciences, Prince Sultan University, Riyadh 11586, Saudi Arabia.

REFERENCES

[1] Banafaa, M., I. Shayea, J. Din, M. H. Azmi, A. Alashbi, Y. I. Daradkeh, and A. Alhammadi, "6G mobile communication technology: Requirements, targets, applications, challenges, advantages, and opportunities," *Alexandria Engineering Journal*, Vol. 64, 245–274, 2023.

[2] Padhi, P. K. and F. Charrua-Santos, "6G enabled industrial internet of everything: Towards a theoretical framework," *Applied System Innovation*, Vol. 4, No. 1, 11, 2021.

[3] Frei, M., T. Deinlein, R. German, and A. Djanatliev, "An evaluation of the communication performance of MEC-dependent services in 5G networks," in *2021 IEEE 20th International Symposium on Network Computing and Applications (NCA)*, 1–8, 2021.

[4] Serghiou, D., M. Khalily, T. W. C. Brown, and R. Tafazolli, "Terahertz channel propagation phenomena, measurement techniques and modeling for 6G wireless communication applications: A survey, open challenges and future research directions," *IEEE Communications Surveys & Tutorials*, Vol. 24, No. 4, 1957–1996, 2022.

[5] Mustafa Hilal, A., J. S. Alzahrani, I. Abunadi, N. Nemri, F. N. Al-Wesabi, A. Motwakel, I. Yaseen, and A. S. Zamani, "Intelligent deep learning model for privacy preserving IIoT on 6G environment," *Computers, Materials & Continua*, Vol. 72, No. 1, 333–348, 2022.

[6] Xu, L., X. Zhou, Y. Tao, X. Yu, M. Yu, and F. Khan, "AF relaying secrecy performance prediction for 6G mobile communication networks in industry 5.0," *IEEE Transactions on Industrial Informatics*, Vol. 18, No. 8, 5485–5493, 2022.

[7] Likas, A., N. Vlassis, and J. J. Verbeek, "The global K-means clustering algorithm," *Pattern Recognition*, Vol. 36, No. 2, 451–461, 2003.

[8] Ali, S., W. Saad, and D. Steinbach, "Machine learning in 6G wireless communication networks," Tech. Rep., Jun. 2020.

[9] IEEE Xplore Digital Library, "How will machine learning redefine wireless communication for 6G?" Sep. 2022.

[10] Iliadis, L. A., Z. D. Zaharis, S. Sotiroudis, P. Sarigiannidis, G. K. Karagiannidis, and S. K. Goudos, "The road to 6G: A comprehensive survey of deep learning applications in cell-free massive MIMO communications systems," *EURASIP Journal on Wireless Communications and Networking*, Vol. 2022, No. 1, 68, Aug. 2022.

[11] Traßl, A., E. Schmitt, T. Hößler, L. Scheuvens, N. Franchi, N. Schwarzenberg, and G. Fettweis, "Outage prediction for ultra-reliable low-latency communications in fast fading channels," *EURASIP Journal on Wireless Communications and Networking*, Vol. 2021, 92, 2021.

[12] Yang, F., D. W. Wanik, D. Cerrai, M. A. E. Bhuiyan, and E. N. Anagnostou, "Quantifying uncertainty in machine learning-based power outage prediction model training: A tool for sustainable storm restoration," *Sustainability*, Vol. 12, No. 4, 1525, 2020.

[13] Khalil, H., S. U. Rahman, I. Ullah, I. Khan, A. J. Alghadhban, M. H. Al-Adhaileh, G. Ali, and M. ElAffendi, "A UAV-swarm-communication model using a machine-learning approach for search-and-rescue applications," *Drones*, Vol. 6, No. 12, 372, 2022.

[14] Tian, H. W., H. Y. Shen, X. G. Zhang, X. Li, W. X. Jiang, and T. J. Cui, "Terahertz metasurfaces: toward multifunctional and programmable wave manipulation," *Frontiers in Physics*, Vol. 8, 584077, 2020.

[15] Zhu, S.-Y., G.-B. Wu, S. W. Pang, and C. H. Chan, "Compact terahertz dielectric folded metasurface," *Advanced Optical Materials*, Vol. 10, No. 3, 2101663, 2021.

[16] Chen, S., J. Zhang, Y. Jin, and B. Ai, "Wireless powered IoE for 6G: Massive access meets scalable cell-free massive MIMO," *China Communications*, Vol. 17, No. 12, 92–109, 2020.

[17] Qadir, Z., K. N. Le, N. Saeed, and H. S. Munawar, "Towards 6G internet of things: Recent advances, use cases, and open challenges," *ICT Express*, Vol. 9, No. 3, 296–312, 2023.

[18] Asim, M., M. ELAffendi, and A. A. A. El-Latif, "Multi-IRS and multi-UAV-assisted MEC system for 5G/6G networks: Efficient joint trajectory optimization and passive beamforming framework," *IEEE Transactions on Intelligent Transportation Systems*, Vol. 24, No. 4, 4553–4564, 2022.

[19] Xiao, Z., Z. Han, A. Nallanathan, O. A. Dobre, B. Clerckx, J. Choi, C. He, and W. Tong, "Antenna array enabled space/air/ground communications and networking for 6G," *IEEE Journal on Selected Areas in Communications*, Vol. 40, No. 10, 2773–2804, 2022.

[20] González-Ovejero, D., C. Jung-Kubiak, M. Alonso-delPino, T. Reck, and G. Chattopadhyay, "Design, fabrication and testing of a modulated metasurface antenna at 300 GHz," in *2017 11th European Conference on Antennas and Propagation (EUCAP)*, 3416–3418, 2017.

[21] Naqvi, S. I. and N. Hussain, "Antennas for 5G and 6G communications," *5G and 6G Enhanced Broadband Communications*, 2022.

[22] Montaser, A. M. and K. R. Mahmoud, "Design of intelligence reflector metasurface using deep learning neural network for 6g adaptive beamforming," *IEEE Access*, Vol. 10, 117 900–117 913, 2022.

[23] Rahman, S. U., Q. Cao, I. Gil, M. Sajjad, and Y. Wang, "Design of wideband beamforming metasurface with alternate absorption," *IEEE Access*, Vol. 8, 21 393–21 400, 2020.

[24] Makin, M., K. Dautov, M. S. Hashmi, T. A. Tsiftsis, and G. Nauryzbayev, "Outage analysis and realization challenges of RIS-enabled underlay CR networks over nakagami — m fading," in *2022 13th International Conference on Information and Communication Technology Convergence (ICTC)*, 193–198, 2022.

[25] Geraci, G., A. Garcia-Rodriguez, M. M. Azari, A. Lozano, M. Mezzavilla, S. Chatzinotas, Y. Chen, S. Rangan, and M. D. Renzo, "What will the future of UAV cellular communications be? A flight from 5G to 6G," *IEEE Communications Surveys & Tutorials*, Vol. 24, No. 3, 1304–1335, 2022.

[26] Chen, G. and G. Chen, "A method of relay node selection for UAV cluster networks based on distance and energy constraints," *Sustainability*, Vol. 14, No. 23, 16089, 2022.

[27] Almasoud, A. S., S. B. H. Hassine, N. Nemri, F. N. Al-Wesabi, M. A. Hamza, A. M. Hilal, A. Motwakel, and M. A. Duhayyim, "Metaheuristic based data gathering scheme for clustered UAVs in 6G communication network," *Computers, Materials & Continua*, Vol. 71, No. 3, 5311–5325, 2022.

[28] Belaoura, W., K. Ghanem, M. Z. Shakir, and M. O. Hasna, "Performance and user association optimization for UAV relay-assisted mm-Wave massive MIMO systems," *IEEE Access*, Vol. 10, 49 611–49 624, 2022.

[29] Liu, C., W. Feng, Y. Chen, C.-X. Wang, and N. Ge, "Cell-free satellite-UAV networks for 6G wide-area internet of things," *IEEE Journal on Selected Areas in Communications*, Vol. 39,

No. 4, 1116–1131, 2021.

[30] Zaidi, A., F. Athley, J. Medbo, U. Gustavsson, G. Durisi, and X. Chen, "Chapter 3 — propagation & channel modeling," 5G Physical Layer, 2018.

[31] Clough, S. A., M. J. Iacono, and J.-L. Moncet, "LBLRTM: Line-by-line radiative transfer model," *Astrophysics Source Code Library, Record Ascl:1405.001*, ascl–1405, May 2014.

[32] Bogale, T. E., X. Wang, and L. B. Le, "MmWave communication enabling techniques for 5G wireless systems: A link level perspective," *MmWave Massive MIMO*, 195–225, S. Mumtaz, J. Rodriguez, and L. Dai (eds.), Elsevier, 2017.

[33] Zubair, M., Z. Haider, S. A. Khan, and J. Nasir, "Atmospheric influences on satellite communications," *Przeglad Elektrotechniczny*, Vol. 87, 2011.

[34] Federici, J. and L. Moeller, "Review of terahertz and subterahertz wireless communications," *Journal of Applied Physics*, Vol. 107, No. 11, 111101, 2010.

[35] Series, P., "Attenuation by atmospheric gases and related effects," *Recommendation ITU-R*, Vol. 25, 676–12, 2019.

[36] Madden, J., "The ideal band for 6G," *Microwave Journal*, Vol. 65, No. 8, Aug. 2022.

[37] Traßl, A., E. Schmitt, T. Hößler, L. Scheuvens, N. Franchi, N. Schwarzenberg, and G. Fettweis, "Outage prediction for ultra-reliable low-latency communications in fast fading channels," *EURASIP Journal on Wireless Communications and Networking*, Vol. 2021, No. 1, 92, Apr. 2021.

[38] Rikkinen, K., P. Kyosti, M. E. Leinonen, M. Berg, and A. Parssinen, "THz radio communication: Link budget analysis toward 6G," *IEEE Communications Magazine*, Vol. 58, No. 11, 22–27, 2020.

[39] Khan, M. A., N. Kumar, S. A. H. Mohsan, W. U. Khan, M. M. Nasralla, M. H. Alsharif, J. Żywiołek, and I. Ullah, "Swarm of UAVs for network management in 6G: A technical review," *IEEE Transactions on Network and Service Management*, Vol. 20, No. 1, 741–761, Mar. 2023.

[40] Wang, X., Y. Guo, and Y. Gao, "Unmanned autonomous intelligent system in 6G non-terrestrial network," *Information*, Vol. 15, No. 1, 38, 2024.

[41] Mustari, N., M. A. Karabulut, A. F. M. S. Shah, and U. Tureli, "Cooperative THz communication for UAVs in 6G and beyond," *Green Energy and Intelligent Transportation*, Vol. 3, No. 1, 100131, 2024.

[42] Zhang, Q., W. Saad, and M. Bennis, "Reflections in the sky: Millimeter wave communication with UAV-carried intelligent reflectors," in *2019 IEEE Global Communications Conference (GLOBECOM)*, 1–6, 2019.

[43] Fang, J., Z. Yang, N. Anjum, Y. Hu, H. Asgari, and M. Shikh-Bahaei, "Secure intelligent reflecting surface assisted UAV communication networks," in *2021 IEEE International Conference on Communications Workshops (ICC Workshops)*, 1–6, 2021.

[44] Arafat, M. Y. and S. Moh, "Localization and clustering based on swarm intelligence in UAV networks for emergency communications," *IEEE Internet of Things Journal*, Vol. 6, No. 5, 8958–8976, 2019.

[45] Rekkas, V. P., S. Sotiroudis, P. Sarigiannidis, S. Wan, G. K. Karagiannidis, and S. K. Goudos, "Machine learning in beyond 5G/6G networks — State-of-the-art and future trends," *Electronics*, Vol. 10, No. 22, 2786, 2021.

[46] Yu, P., F. Zhou, T. Zhang, W. Li, L. Feng, and X. Qiu, "Self-organized cell outage detection architecture and approach for 5G H-CRAN," *Wireless Communications and Mobile Computing*, Vol. 2018, 6201386, 2018.

[47] Shlezinger, N., G. C. Alexandropoulos, M. F. Imani, Y. C. Eldar, and D. R. Smith, "Dynamic metasurface antennas for 6G extreme massive MIMO communications," *IEEE Wireless Communications*, Vol. 28, No. 2, 106–113, 2021.

[48] Liu, G., N. Li, J. Deng, Y. Wang, J. Sun, and Y. Huang, "The SOLIDS 6G mobile network architecture: Driving forces, features, and functional topology," *Engineering*, Vol. 8, 42–59, 2022.

[49] Mao, B., Y. Kawamoto, and N. Kato, "AI-based joint optimization of QoS and security for 6G energy harvesting Internet of Things," *IEEE Internet of Things Journal*, Vol. 7, No. 8, 7032–7042, 2020.

[50] Khan, M. A., N. Kumar, S. A. H. Mohsan, W. U. Khan, M. M. Nasralla, M. H. Alsharif, J. Żywiołek, and I. Ullah, "Swarm of UAVs for network management in 6G: A technical review," *IEEE Transactions on Network and Service Management*, Vol. 20, No. 1, 741–761, 2023.